J. Fluid Mech. (1985), *vol.* 150, *pp.* 1–21
Printed in Great Britain

Laminar flow through a slowly rotating straight pipe

By KAMYAR MANSOUR
Department of Aeronautics and Astronautics, Stanford University, California, 94305

(Received 17 February 1983 and in revised form 31 January 1984)

We consider fully developed steady laminar flow through a pipe that is rotating slowly about a line perpendicular to its own axis. The solution is expanded for low Reynolds numbers in powers of a single combined similarity parameter and the series extended to 34 terms by computer. Analysis shows that convergence is limited by a square-root singularity on the negative real axis of the similarity parameter. An Euler transformation and extraction of the leading, secondary and tertiary singularities at infinity render the series accurate for all values of the similarity parameter. The major conclusion of this investigation is that the friction ratio in a slowly rotating pipe grows asymptotically as the $\frac{1}{8}$ power of the similarity parameter and not as the $\frac{1}{4}$ power as previously deduced from boundary-layer analysis. This discrepancy between the present computer-extended method and boundary-layer analysis has also occurred in the similar problem of flow through a loosely coiled pipe (Van Dyke 1978).

1. Introduction

This work is concerned with the problem of flow through a pipe that is rotating about a line perpendicular to its own axis. The goal of the analysis is to provide as complete a description as possible of the flow. Even though the problem involves two parameters, it turns out that an adequate solution can be obtained in terms of a single combined similarity parameter.

Previous work on this problem has been modelled on the pioneering theoretical analysis of Dean (1927, 1928) and the experiments of White (1929) and Adler (1934) for the analogous problem of a coiled pipe. Thus Barua (1954) followed Dean in perturbing the Poiseuille flow by expanding the cross-flow stream function and axial velocity in double power series in two parameters that are combinations of the Reynolds numbers R and R_r, based on the axial and rotational velocities. He obtained an expansion for the friction ratio in terms of the same two parameters. Independently, Benton (1956) also made a small-perturbation analysis based on the Poiseuille flow, and carried out experiments showing the effect of the Earth's rotation on laminar flow in a pipe. His solution is qualitative in nature. A somewhat different approach to the problem has been adopted by Jones & Walters (1967); they neglect the boundary layer at the wall, assume uniform flow in the core, find the axial-velocity distribution, and are thereby able to obtain the flow rate. Their results confirm Barua's conclusion that the flow rate is less than that for the corresponding flow in a stationary pipe under the same pressure gradient. Furthermore, Itō & Motai (1974) considered simultaneously in a single paper the effects of both curving and rotating a pipe. Their double expansion reproduces the result obtained separately by Dean and Barua.

The first experiments for a rotating pipe were conducted by Trefethen (1957*a*, *b*). The most important part of his observation was that the onset of turbulence is

inhibited by rotation of the pipe. Secondly, he found that for a slowly rotating pipe the laminar regime can be correlated by a single similarity parameter $K = RR_r$. More recently, Itō & Nanbo (1970) performed experiments to find the friction factor, velocity distribution in the piane of symmetry, and pressure distribution along the circumferential wall of the pipe.

The first boundary-layer analysis of this problem was made by Mori & Nakayama (1968). They assumed that the boundary-layer thickness is constant with respect to the angular coordinate inasmuch as the Coriolis force due to the rotation acts in a fixed direction. Their assumption about angular independence of the thickness seems unreasonable. Itō & Nanbo (1970) also carried out a boundary-layer analysis. Their equations were solved via the Kármán–Polhausen method of integration. But their model seems to be invalid in the vicinity of the innermost ring because at that point they predict infinite boundary-layer thickness.

For the problem of flow through a loosely coiled pipe, Dean (1927) was able to express the solution to a good approximation in terms of a single expansion parameter that now bears his name. However, for the rotating-pipe problem, neither Barua (1954) nor Benton (1956) was able to expand the solution in terms of a single parameter. Consequently, Barua was unable to give the range of validity of the solution, as Dean (1938) did in his curved-pipe research.

The present investigation is a description of how the rotating-pipe problem can theoretically be treated with a single similarity parameter $K = RR_r$. The perturbation expansion is here carried to higher order by delegating the laborious arithmetic to a computer. In many papers, Van Dyke has exploited this method for unveiling the structure of various flows in fluid mechanics (see Van Dyke 1975). We note that in many problems the structure of the boundary layer is complicated, possibly due to colliding layers, internal jets and/or flow separation. One way to overcome such a difficulty is to apply seminumerical methods.†

The problem under present consideration, the slowly rotating pipe, is one of those simple, experimentally realizable and realistic problems where this technique can be examined. In contrast with boundary-layer techniques, the seminumerical methods make no assumption as to the nature of the core when K is infinite.

2. Statement of problem

We consider the steady fully developed laminar flow through a pipe of circular cross-section that is rotating with a constant angular velocity about a line perpendicular to its axis (figure 1). This problem was first analysed by Barua (1954). For clarification we modify Barua's dimensionless Navier–Stokes equations so that the dependent as well as the independent variables are of order unity for slow rotation. This requires referring lengths to the radius a of the pipe, as usual, but referring the axial velocity W to Dean's (1928) W_0 (the maximum speed in Poiseuille flow through the non-rotating pipe under the same pressure gradient) rather than to ν/a, and referring the cross-flow stream function Ψ to $2\Omega W_0 a^3/\nu$ rather than to ν. Then the dimensionless problem becomes

$$\nabla^2 W + 4 = RR_r \frac{1}{r}\left(\frac{\partial \Psi}{\partial \Theta}\frac{\partial W}{\partial r} - \frac{\partial \Psi}{\partial r}\frac{\partial W}{\partial \Theta}\right) + R_r^2\left(\sin\Theta\frac{\partial \Psi}{\partial r} + \frac{\cos\Theta}{r}\frac{\partial \Psi}{\partial \Theta}\right), \tag{2.1}$$

$$\nabla^4 \Psi + \left(\sin\Theta\frac{\partial W}{\partial r} + \frac{\cos\Theta}{r}\frac{\partial W}{\partial \Theta}\right) = RR_r \frac{1}{r}\left(\frac{\partial \Psi}{\partial \Theta}\frac{\partial}{\partial r} - \frac{\partial \Psi}{\partial r}\frac{\partial}{\partial \Theta}\right)\nabla^2 \Psi, \tag{2.2}$$

† This method includes our present technique.

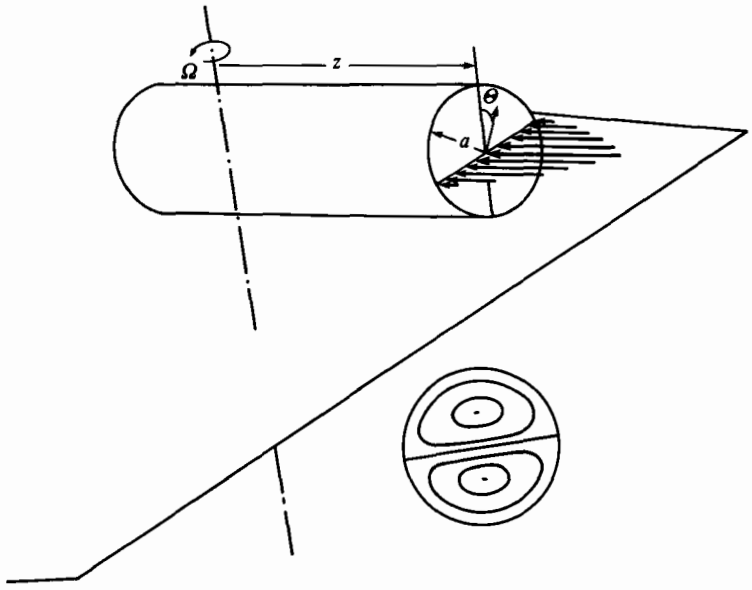

FIGURE 1. Notation for slowly rotating pipe.

where $$\nabla^2 = \frac{\partial^2}{\partial r^2} + \frac{1}{r}\left(\frac{\partial}{\partial r}\right) + \frac{1}{r^2}\left(\frac{\partial^2}{\partial \Theta^2}\right), \quad R = \frac{W_0 a}{\nu}, \quad R_\mathrm{r} = \frac{2a^2\Omega}{\nu}.$$

These equations are to be solved with the boundary conditions

$$W = \Psi = \frac{\partial \Psi}{\partial r} = 0 \quad \text{at} \quad r = 1.$$

3. Slow rotation

3.1. *Analytical solution for slow rotation, $R_\mathrm{r}/R \ll 1$*

Barua (1934) and Benton (1956) attacked this problem by making a double expansion in powers of RR_r and R_r^2 (They used these two parameters, but in different form and notation.) If the problem lends itself to a single expansion then one of the parameters must be related to the other by considering a double-limit process. By analogy with Dean's treatment of the flow through a curved pipe, one can analyse the double limit†

$$\left.\begin{matrix} R_\mathrm{r} \to 0, \\ R \to \infty, \end{matrix}\right\} \quad K = RR_\mathrm{r} \text{ fixed}.$$

Under this limiting process, which we call slow rotation, the last term disappears from (2.1); then the equations reduce to

$$\nabla^2 W + 4 = K\frac{1}{r}\left(\frac{\partial \Psi}{\partial \Theta}\frac{\partial W}{\partial r} - \frac{\partial \Psi}{\partial r}\frac{\partial W}{\partial \Theta}\right), \tag{3.1}$$

$$\nabla^4 \Psi + \left(\sin\theta \frac{\partial W}{\partial r} + \frac{\cos\theta}{r}\frac{\partial W}{\partial \Theta}\right) = K\frac{1}{r}\left(\frac{\partial \Psi}{\partial \Theta}\frac{\partial}{\partial r} - \frac{\partial \Psi}{\partial r}\frac{\partial}{\partial \Theta}\right)\nabla^2 \Psi, \tag{3.2}$$

with $$W = \Psi = \frac{\partial \Psi}{\partial r} = 0 \quad \text{at} \quad r = 1. \tag{3.3}$$

If the pipe is rotating slowly, or the rotational Reynolds number R_r is small, so that

† The explanation of this particular combination $K = RR_\mathrm{r}$ is given in the Appendix.

K is small, the nonlinear terms on the right-hand side of (2.1) are negligible and the first approximation is the familiar Poiseuille flow, with

$$W_1 = 1-r^2. \tag{3.4}$$

One can systematically improve on this approximation by expanding in powers of K according to

$$\left.\begin{aligned} W &= W_1+KW_2+K^2W_3+\ldots = \sum_1^\infty K^{n-1}W_n, \\ \Psi &= \Psi_1+K\Psi_2+K^2\Psi_3+\ldots = \sum_1^\infty K^{n-1}\Psi_n. \end{aligned}\right\} \tag{3.5}$$

Substituting (3.5) into (3.1) and (3.2) and equating like powers of K yields the sequence of linear equations

$$\nabla^2 W_n = \left\{\begin{array}{c} -4 \quad (n=1), \\ \frac{1}{r}\sum_1^n\left(-\frac{\partial\Psi_j}{\partial r}\frac{\partial W_{n-j}}{\partial\Theta}+\frac{\partial\Psi_j}{\partial\Theta}\frac{\partial W_{n-j}}{\partial r}\right) \quad (n\neq 1), \end{array}\right\} \tag{3.6}$$

$$\nabla^4\Psi_n = \left\{\begin{array}{c} \frac{1}{r}\left(r\sin\Theta\frac{\partial W_1}{\partial r}+\cos\Theta\frac{\partial W_1}{\partial\Theta}\right) \quad (n=1), \\ \frac{1}{r}\sum_1^n\left(-\frac{\partial\Psi_j}{\partial r}\frac{\partial}{\partial\Theta}+\frac{\partial\Psi_j}{\partial\Theta}\frac{\partial}{\partial r}\right)\nabla^2\Psi_{n-j}-\frac{1}{r}\left(r\sin\theta\frac{\partial W_n}{\partial r}+\cos\Theta\frac{\partial W_n}{\partial\Theta}\right) \quad (n\neq 1), \end{array}\right\} \tag{3.7}$$

with boundary conditions

$$W_n = \Psi_n = \frac{\partial\Psi_n}{\partial r} = 0 \quad \text{at} \quad r=1. \tag{3.8}$$

These equations can be solved by separating variables in coordinates r and Θ. Thus we find

$$W = 1-r^2+\tfrac{1}{768}K(r-2r^3+\tfrac{4}{3}r^5-\tfrac{1}{3}r^7)\cos\Theta+\ldots, \tag{3.9}$$

$$\Psi = \tfrac{1}{768}(8r-16r^3+8r^5)\sin\Theta+\ldots. \tag{3.10}$$

The difficulty of successively finding the higher-order terms rapidly becomes greater. Barua (1954) was able to calculate one more term in each of the series (3.9), (3.10) as Dean did for his own loosely curved pipe. Independently of Barua (1954), and with a different form of expansion, Benton (1956) has also given results up to the second approximation (order of K^2) in each of these series. From the series solution we can compute two related global quantities of practical interest. The flux ratio is defined as the ratio of the flux F_r through a rotating pipe to the flux F_s through a stationary pipe with the same pressure gradient. Its series has the form

$$\frac{F_r}{F_s} = \sum_0^\infty a_n\left(\frac{K}{768}\right)^{2n} = 1-\frac{1}{7}\left(\frac{K}{768}\right)^2+\ldots. \tag{3.11}$$

Alternatively, Itō & Nanbu (1970) define the friction ratio as

$$\left(\frac{F_r}{F_s}\right)^{-1} = \sum_0^\infty b_n\left(\frac{K}{768}\right)^{2n} = 1+\frac{1}{7}\left(\frac{K}{768}\right)^2+\ldots. \tag{3.12}$$

The numerical coefficients of the flux-ratio series (3.11) are in good agreement with the result obtained by Barua. It is worth mentioning that the numerical coefficients of the friction-ratio series (3.12) do not match with Barua's corresponding coefficients because he used a different definition of friction ratio.

3.2. *Experimental observations*

Some remarkable experimental observations have been made regarding the secondary motion induced by external forces in flow through a pipe. In the three different cases of flow in a rotating pipe, in a curved pipe and in a horizontal heated pipe, the same phenomenon of double helical motion has occurred. This helical motion stabilizes the flow, and so delays the onset of turbulence until a higher value of the Reynolds number than for the corresponding pipe with no external force.

White (1929) was the first to discover that bending a pipe to a radius ratio $a/R = \frac{1}{15}$ (radius of the pipe, divided by radius of curvature) increases the critical Reynolds number (based on mean flow speed) from about 2300 to 7800. Similarly Trefethen (1957*a*,*b*) has confirmed the inhibition of the onset of turbulence and resulting stabilization of flow in a curved pipe, as well as in a rotating or heated horizontal pipe.

In the case of flow through a rotating pipe, Itō (1970) has discovered that, for a pipe at $R_r = 2000$ (Reynolds number based on angular velocity), the critical Reynolds number (based on mean-flow speed) is almost three times the corresponding critical Reynolds number in a straight pipe. As a result of Ito's (1970) experiments, it can be anticipated that the laminar regime will persist beyond $K = 10^7$ for $R_r \approx 2000$.

Equation (3.11) is the result of solving the problem of flow through a rotating pipe while assuming low value of K. We find in §3.3 that the series (3.11) converges only up to $K = 413$ (which corresponds to Itō's similarity parameter $k = 790$, where k is defined in §5.1. This value will be computed in §3.3. Inasmuch as Itō's experiments have shown that the laminar region extends beyond $K = 10^7$, the following sections explain how to increase the range of validity of the series solution to cover the whole laminar range.

3.3. *Computer extension*

In recent years, the field of computational fluid dynamics has developed sufficiently to demand changes in traditional methods of flow calculation. The powers of both computers and numerical algorithms (mainly finite differences or, increasingly, finite elements) are simultaneously improving with time. However, some fluid mechanicians cannot believe that these techniques alone will continue into the next century. Other methods will surely be developed that more effectively employ the remarkable capabilities of the digital computer.

A likely possibility is the semi-analytical numerical technique of computer extension. In brief form, it consists of extending a regular perturbation expansion to higher order by delegating the mounting arithmetic to a computer, then analysing the structure of the solution in the complex plane of the perturbation quantity, and on that basis improving the utility of the series. Of course, the choice of problems is limited by the requirement that the extension be a regular perturbation, since there is no simple scheme for analysing and improving the asymptotic expansion corresponding to a singular perturbation. In this technique it is essential first to calculate several terms by hand, in order to find the pattern for writing recursion relations for the successive terms of the series, and to aid in debugging a computer program. The limited accuracy of floating-point numbers will be controlled by running in both double and quadruple precision. A program consists mainly of nested DO loops. For the particular problem of flow in a rotating pipe, the difficulty of floating-point underflow will be avoided by scaling down the expansion parameter

K, and correspondingly scaling up the ratios of successive W_n, Ψ_n by a scale factor S, here taken as 768:

$$\overline{W}_n = \frac{W_n}{S^{n-1}}, \quad \overline{\Psi}_n = \frac{\Psi_n}{S^{n-1}}, \quad \overline{K} = SK. \tag{3.13}$$

Then our general expansions (3.5) and (3.5) are changed to

$$W = \sum_{1}^{\infty} \overline{K}^{n-1}\, \overline{W}_n, \quad \Psi = \sum_{1}^{\infty} \overline{K}^{n-1}\, \overline{\Psi}_n. \tag{3.14}$$

By induction, we find that the functions W_n and Ψ_n depend upon the coordinates as follows (with the bars omitted):

$$\Psi_n = \sum_{i=1}^{\frac{1}{2}(n+1)} \sum_{j=1}^{2n+1} C_{nij} r^{5n+2-2j} \sin{(n+2-2i)\,\Theta}, \tag{3.15}$$

$$W_n = \sum_{i=1}^{\frac{1}{2}(n+1)} \sum_{j=1}^{2n+i-1} E_{nij} r^{5n+2-2j} \sin{(n+2-2i)\,\Theta}, \quad n = 1, 2, 3, \ldots. \tag{3.16}$$

A Fortran program of some 500 statements was written that successively calculates the coefficients C_{nij} and E_{nij} in these expressions. The program consists mainly of DO loops nested five deep, so that the computer time increases almost as the fifth power of the number of the terms. An IBM 370/3081 computer was used for the numerics. Eleven minutes of calculation yielded the solution (3.14) up to $n = 34$, and therefore 17 terms for (3.11) and (3.12) in quadruple precision. Computer core-size limitations are important, as about 700000 bytes are required for the 34-term computation. Most of this large storage requirement is because of nonlinear terms involved in the original differential equations. Although the coefficients C_{nij}, E_{nij}, etc. are all rational fractions, we compute them as truncated decimals, so that errors accumulate. Comparison of a double- and quadruple-precision computation shows that not quite one significant figure is lost from these coefficients as the order of approximation n increases by two. The IBM 370/3081 has the advantage of providing 32 significant figures in quadruple precision, so we know that our 34 coefficients are all correct up to 16 figures. The coefficients a_n and b_n in the series (3.11) and (3.12) for the flux and friction ratios are listed to 10 decimal places in table 1.

3.4. *Radius of convergence*

The range in which a series can be useful in practical computation is limited by the nearest singularity. That singularity is often a simple pole or branch point, which is located (in general) in the complex plane of the expansion variable ($RR_r = K$, in this case).

Domb–Sykes plot

If the nearest singularity is on the real axis, then for estimating the radius of convergence one can use a simple graphical test due to Domb & Sykes (1957). The coefficients a_n in (3.11) are seen in table 1 to alternate regularly in sign, which shows that the nearest singularity lies on the negative real axis of $(K/768)^2$. If this singularity is an algebraic branch point of exponent α, that is, behaves locally like

$$f(K) = \text{constant} + \text{constant}\left(1 + \frac{(K/768)^2}{D}\right)^{\alpha} + \ldots, \quad \text{as} \quad (K/768)^2 \to -D, \tag{3.17}$$

	a_n	b_n	c_n	d_n
1	1.000000000	1.000000000	1.00000000	1.000000000
2	$-1.428571423\times10^{-1}$	1.428571428×10^{-1}	-4.13757476×10^{-2}	4.137574763×10^{-2}
3	2.082649930×10^{-1}	$-1.878568298\times10^{-1}$	-2.39052937×10^{-2}	2.561725120×10^{-2}
4	$-4.185257732\times10^{-1}$	3.619369413×10^{-1}	-1.66032794×10^{-2}	1.865231200×10^{-2}
5	9.724698814×10^{-1}	$-8.218512065\times10^{-1}$	-1.26266080×10^{-2}	1.469772256×10^{-2}
6	-2.456050351	2.045717048	-1.01378094×10^{-2}	1.213959352×10^{-2}
7	6.548607567	-5.400170055	-8.43945624×10^{-3}	1.034570243×10^{-2}
8	-1.813939041×10^{1}	1.484904641×10^{1}	-7.20981073×10^{-3}	9.016509972×10^{-3}
9	5.168760899×10^{1}	-4.207576191×10^{1}	-6.28027144×10^{-3}	7.991393408×10^{-3}
10	-1.505343927×10^{2}	1.220012810×10^{2}	-5.55411902×10^{-3}	7.176330285×10^{-3}
11	4.460970700×10^{2}	-3.602527317×10^{2}	-4.97197772×10^{-3}	6.512553594×10^{-3}
12	-1.340811093×10^{3}	1.079605490×10^{3}	-4.49542048×10^{-3}	5.961410117×10^{-3}
13	4.077628093×10^{3}	-3.275140653×10^{4}	-4.09850230×10^{-3}	5.496416021×10^{-3}
14	-1.252424641×10^{4}	1.003825803×10^{4}	-3.76308659×10^{-3}	5.098807526×10^{-3}
15	3.879497562×10^{4}	-3.103795689×10^{4}	-3.47612180×10^{-3}	4.754913467×10^{-3}
16	-1.210547509×10^{5}	9.669685128×10^{4}	-3.22798151×10^{-3}	4.454534084×10^{-3}
17	3.801612027×10^{5}	-3.032456177×10^{5}	-3.01141378×10^{-3}	4.189902958×10^{-3}

	e_n	f_n	g_n
1	1.000000000	$-1.605790000\times10^{-2}$	$-1.605790000\times10^{-2}$
2	1.417980792×10^{-2}	$-1.915352629\times10^{-2}$	$-9.915352541\times10^{-2}$
3	3.117036298×10^{-3}	1.978370277×10^{-2}	1.397837029×10^{-1}
4	9.457769375×10^{-4}	6.501332417×10^{-3}	$-2.016533417\times10^{-2}$
5	2.655709024×10^{-4}	3.043348641×10^{-3}	$-3.623317986\times10^{-3}$
6	6.568270800×10^{-6}	1.673234915×10^{-3}	$-9.934317291\times10^{-4}$
7	$-9.983598583\times10^{-5}$	1.011275111×10^{-3}	$-3.220582080\times10^{-4}$
8	$-1.425280710\times10^{-4}$	6.511227142×10^{-4}	$-1.107820392\times10^{-4}$
9	$-1.562997036\times10^{-4}$	4.389383862×10^{-4}	$-3.725208464\times10^{-5}$
10	$-1.563717961\times10^{-4}$	3.065911636×10^{-4}	$-1.086915066\times10^{-5}$
11	$-1.499313321\times10^{-4}$	2.204390364×10^{-4}	$-1.783184003\times10^{-6}$
12	$-1.405517701\times10^{-4}$	1.624785320×10^{-4}	8.623712355×10^{-7}
13	$-1.300669304\times10^{-4}$	1.224582719×10^{-4}	1.246150851×10^{-6}
14	$-1.194296294\times10^{-4}$	9.424558450×10^{-5}	1.005490936×10^{-6}
15	$-1.091289492\times10^{-4}$	7.402123454×10^{-5}	7.611606081×10^{-7}
16	$-9.940405691\times10^{-5}$	5.932610272×10^{-5}	7.180432026×10^{-7}
17	$-9.035709599\times10^{-5}$	4.853179398×10^{-5}	9.127452727×10^{-7}

TABLE 1. Coefficients of flux-ratio series

then the ratio a_n/a_{n-1} of successive coefficients will be linear in $1/n$ for large n:

$$\frac{a_n}{a_{n-1}} \approx \frac{1}{D}\left(1-\frac{1+\alpha}{n}+O\left(\frac{1}{n^2}\right)+\ldots\right). \tag{3.18}$$

Therefore, in a plot of a_n/a_{n-1} versus $1/n$, the intercept on the axis of $1/n$ gives the reciprocal of the radius of convergence D, and the intercept on the axis of a_n/a_{n-1} indicates the exponent α. In other words,

$$\lim \frac{a_n}{a_{n-1}} = \frac{1}{D} \quad \text{as} \quad \frac{1}{n}\to 0,$$

$$\lim \frac{\mathrm{d}(a_n/a_{n-1})}{\mathrm{d}(1/n)} = -\frac{1+\alpha}{D} \quad \text{as} \quad \frac{1}{n}\to 0.$$

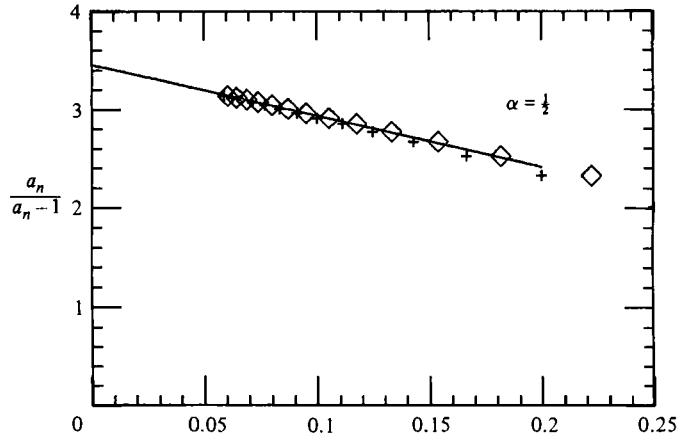

FIGURE 2. Domb–Sykes plot for extended flux-ratio series: +, plotted versus $1/n$; ◇, plotted versus $1/(n-\frac{1}{2})$; ——, asymptote with $\alpha = \frac{1}{2}$.

Figure 2 shows the Domb–Sykes plot for the flux-ratio series (3.11). It also indicates that the plot is remarkably straightened by a shift of $\frac{1}{2}$ in n. Such a shift is admissible because as $n \to \infty$ the change will be of order $1/n^2$ in (3.18). The straight line has a vertical intercept at approximately $1/D = 3.45$ ($(K/768)^2 = 1/3.45$). The slope clearly indicates the presence of a square-root singularity; i.e. a square-root branch point on the negative real axis of K^2. This corresponds to a conjugate pair of square-root singularities lying on the imaginary axis of the similarity variable K itself. Thus the nearest singularity has no physical significance and unnecessarily limits the range of applicability of the series.

Neville tables

In order to improve our estimate for the radius of convergence, we fit a polynomial of degree M in $1/(n-\frac{1}{2})$ to all the sets of $M+1$ consecutive points in figure 2, and compute the intercept at $1/n = 0$. This can be done by forming a Neville table of the successive ratios of coefficients a_n/a_{n-1} as discussed by Gaunt & Guttman (1974). The first column of this table consists of the ordinates of the points of the Domb–Sykes plot (figure 2). The elements of the rth column are generated from the $(r-1)$th by:

$$e(n,r) = \frac{n\,e(n,r-1) - (n-r)\,e(n-1,r-1)}{r}.$$

The $e(n,2)$ are the linear intercepts from two points, the $e(n,3)$ the quadratic intercepts from three, etc. The entries in column $e(n,8)$ give for the reciprocal of the radius of convergence:

3.451268125, 3.452698826, 3.452716943, 3.452697903, 3.452685765,
3.452680736, 3.452678965, 3.452678399, 3.452678236, ...

This sequence evidently converges to a value 3.4526782. A corresponding Neville table for finding the exponent α can be formed by letting $e(n,2)$ be the slopes through the successive points in figure 2. This confirms the value of $\frac{1}{2}$ for the exponent of the nearest singularity.

Modified Domb–Sykes plot

To refine further the value of the radius of convergence D, we use the known value $\alpha = \frac{1}{2}$ of the exponent to fit a polynomial

$$G\left(\frac{1}{n}\right) = \frac{1}{D}\left(1 - \frac{1+\alpha}{n} + \frac{X(1)}{n^2} + \frac{X(2)}{n^3} + \ldots\right) \tag{3.19}$$

to the Domb–Sykes ratios $a_2/a_1, a_3/a_2, \ldots, a_n/a_{n-1}$ with exponent α and with n shifted upward by $\frac{1}{2}$. This gives the following sequence of numbers as the final values in each column of the Neville table:

3.452681882, 3.452678267, 3.452678317, 3.452678201, 3.452678222,
3.452678232, 3.452678226, 3.452678222, 3.452678223, 3.452678223,
3.452678224, 3.452678225, 3.452678224, 3.452678224, 3.452678224, ...

This seems to converge to a value for $1/D = 3.452678224$. Therefore we find that the series (3.11) converges up to $(K/768)^2 = 1/3.452678224$ or $K = 413.3169036$.

Remarks about convergence

Any other quantity, either local or global, has the same radius of convergence as the flux ratio, but may have a different exponent than $\frac{1}{2}$ since it is the result of integration or differentiation of the original quantities. This was confirmed by considering the series for the following:

(a) the vorticity at the point that is located in the vertical line at $r = 0.5$;

(b) the transverse skin friction at the top of the pipe;

(c) the axial velocity down the centre of the pipe.

For each of these quantities all the usual devices, such as a Domb–Sykes plot or Neville table, give the same radius of convergence. We remark that a point quantity, such as the velocity at any arbitrary location inside the cross-sectional plane, is in general a function of odd as well as even powers of the similarity parameter K. Thus it has a pair of complex-congugate singularities at $(D)^{\frac{1}{2}}$ and $-(D)^{\frac{1}{2}}$ on the imaginary axis of the plane of $K/768$; it must be treated as having a complex pair of singularities rather than a single singularity on the negative real axis.

The functional representation of the flux-ratio series

After we identify the nearest singularities (at least approximately) in the complex plane of the perturbation quantity K, or partially unveil the analytic structure of the solution, the question will arise as to how this knowledge can be exploited to extend the range of validity to improve the utility of the series. There are several possibilities depending on whether the first singularity is of multiplicative or additive type, as discussed by Van Dyke (1974). By forming a new series

$$\left(1 + \frac{(K/768)^2}{D}\right)^{\frac{1}{2}} \frac{F_r}{F_s},$$

we find that the extracted series has a singularity at the same location with an exponent $+\frac{1}{2}$. This shows that the first singularity is of additive, rather than multiplicative, type. As indicated by (3.17), this is the usual situation. Then the singularity must be extracted by subtraction, which requires an estimate of its magnitude. When the first singularity is subtracted, the new series has a singularity at the same location with exponent $\pm\frac{3}{2}$. This process of subtracting out singularities can be continued as far as the accuracy allows.

Forming Padé approximants (Baker 1965), we can conclude that in addition to the singularity on the negative real axis of K^2 there is only a singularity at infinity. That is, applying Padé approximants of different order shows one fixed pole, which is the nearest singularity, and many other poles, all of which are located on the negative real axis. It is important to mention that the other poles all move toward these two singularities as the degree of the denominator is increased. This behaviour is explained by the fact that a Padé approximant is single-valued and therefore needs to introduce a branch cut joining the singularities, which it simulates as a series of poles.

Although we now know the location of the only two singularities in the plane of K^2, it is still tedious to extract the behaviour near the singularity at infinity.

3.5. *Extension of the range of validity*

The nearest singularity is on the negative real axis of K^2, has no physical significance, and therefore unnecessarily limits the range of applicability of the series. As previously mentioned, there are several possible ways in which the radius of convergence can be extended (see Van Dyke 1974; Gaunt & Guttmann 1974), depending on the nature of the singularity.

Euler transformation

An Euler transformation is one way to analytically continue a series or extend the range of convergence for physical K. We use the new parameter δ defined by

$$\delta = \frac{(K/768)^2}{(K/768)^2 + D}, \tag{3.20}$$

which maps the nearest singularity away to infinity. The new series is given by:

$$\frac{F_r}{F_s} = \sum_1^\infty c_n \delta^n. \tag{3.21}$$

The coefficients c_n for $n = 1, \ldots, 17$ are given in table 1. The transformed series has fixed signs, indicating that the nearest singularity is on the positive real axis of δ. As can be seen in figure 3, points of a new Domb–Sykes plot are well behaved. Therefore the Neville table and the other usual devices previously presented for finding the nature and location of a singularity can be employed to determine its exponent and corresponding radius of convergence. The Domb–Sykes plots of figure 3 clearly indicate that the radius of convergence is equal to one. This nearest singularity at $\delta = 1$ corresponds to $K^2 = \infty$ in the original variables. Thus we have been successful in extending the series up to an infinite value of the similarity parameter $K = RR_r$. A singularity at $\delta = 1$ is confirmed by the associated Neville tables and other available devices.

The exponent at infinity

Estimation of the exponent α of the singularity at $K = \infty$ is the most important part of the analysis. In previous problems, this step has proven to be the hardest, and care must be taken. The Domb–Sykes plot shown in figure 3 is clearly nearly linear, and suggests that the series converges for $0 \leqslant \delta \leqslant 1$ with a limiting singularity of the form

$$\frac{F_r}{F_s} \sim C(1-\delta)^\alpha \quad \text{as} \quad \delta \to 1, \tag{3.22}$$

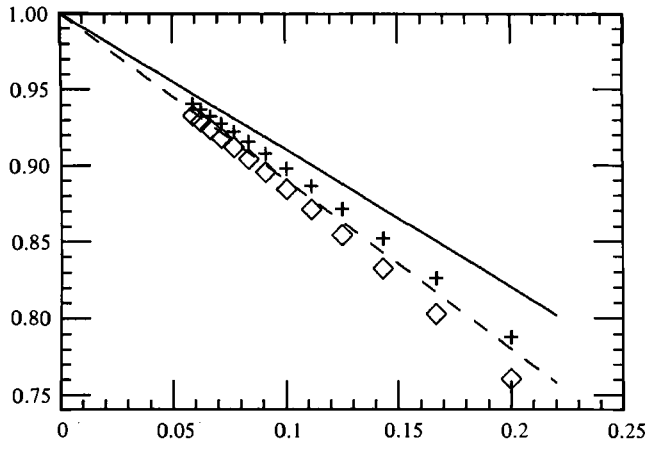

FIGURE 3. Domb–Sykes plots for flux = ratio series after Euler transformation: ◇, direct series; +, inverse series; – – – – –, asymptote for $\alpha = \frac{1}{10}$; ——, asymptote for $\alpha = -\frac{1}{10}$.

which corresponds, in the original parameter, to

$$\frac{F_r}{F_s} \sim cK^{-2\alpha} \quad \text{as} \quad K \to \infty. \tag{3.23}$$

Here α and c are the important parameters that we seek. We try to find the value of α as accurately as possible. The simplest way to estimate α is from the Domb–Sykes plot. Figure 3 implies that its value is very small; we show the terminal slopes for direct and inverse series with $\alpha = \frac{1}{10}$, which is the value according to Itō's boundary-layer model. The corresponding Neville table has an irregular behaviour and does not suggest any value for its magnitude.

A second way, which is one of the most reliable devices, is to take the logarithmic derivative of the series (3.21). Comparing this with the expansion of $\mathrm{d}(\log(1-\delta)^{\alpha})/\mathrm{d}\delta$ yields the following sequence of estimates for α:

0.0413757485, 0.0495225502, 0.0528479707, 0.0545638811, 0.0555468732,
0.0561619310, 0.0565449374, 0.0567876925, 0.0569384331, 0.0570266773,
0.0570713882, 0.0570852224, 0.0570706890, 0.0570525384, 0.0570165919,
0.0569722924, ...

Except for the first three, these are fitted to within 1 % by

$$\alpha \approx \frac{1}{18}\left(1 + \frac{1}{30}\frac{1}{n} - \frac{4}{25}\frac{1}{n(n-1)}\right). \tag{3.24}$$

Figure 4 is the plot of this sequence versus $1/n$. A likely candidate for the intercept is evidently $\frac{1}{18}$. An important feature is a maximum in the plotted points, which indicates that the exponent $\frac{1}{10}$ of the boundary-layer literature cannot be achieved. Furthermore the final entries in each column of the Neville table give the following numbers:

0.053171218, 0.053264697, 0.053398922, 0.053550331, 0.053703981,
0.053850252, 0.053982863, 0.054097677, 0.054191959, 0.054263914, ...

Although the rate of convergence of this sequence is slow, our choice of $\frac{1}{18}$ for the exponent is certainly reasonable.

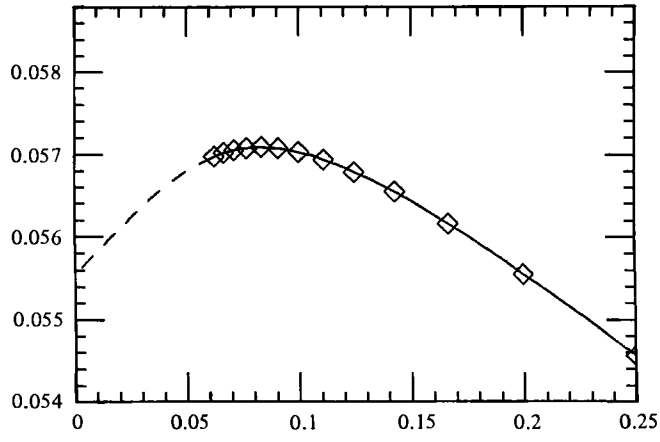

FIGURE 4. Plot for logarithmic derivative after Euler transformation versus $1/n$: ----, (3.24); ——, graphical fit.

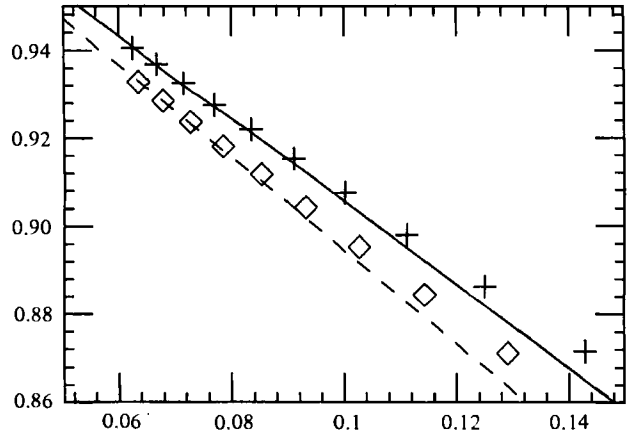

FIGURE 5. Magnified Domb–Sykes plots: ◇, direct series versus $1/(n-1.25)$; +, inverse series versus $1/(n-1)$; ——, asymptote for $\alpha = \frac{1}{18}$; – – – –, asymptote for $\alpha = -\frac{1}{18}$.

Figure 5 is the magnified Domb–Sykes plot of the Euler-transformed series, which also allows the possibility that the exponent is $\alpha \approx \frac{1}{18}$.

A third way to find α is to apply the technique of critical-point renormalization (Gaunt & Guttmann 1974) to the direct and reciprocal series. This yields the following sequence of values for α:

0.06890050, 0.06826510, 0.06735861, 0.06640898, 0.06548528,
0.06460670, 0.06377676, 0.06299366, 0.06225436, 0.06155564,
0.06108844, 0.06026821, 0.05967446, ...

The convergence is so slow that we can only say that the sequence may approach the value $\alpha = 0.0555555$.

A fourth approach involves estimating the value of α by completing the series (see Van Dyke 1974) on the assumption that the value of the multiplicative constant C in $C(1-\delta)^{\alpha}$ can be found by successively equating like terms in the Taylor series expansion with those in the Euler-transformed series (3.21). Figure 6 is the plot of

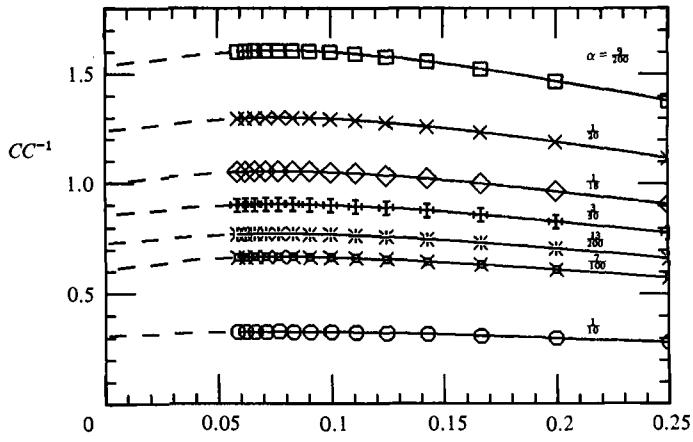

FIGURE 6. Extrapolation of product of completion coefficients for direct and inverse series versus $1/n$.

CC^{-1} versus $1/n$ for different exponents α, where C^{-1} is the corresponding constant for the inverse of the $C(1-\delta)^{\alpha}$ series. This product of completion coefficients must extrapolate to one as n goes to ∞. This figure shows that, better than any other simple rational exponent, the choice $\frac{1}{18}$ can be extrapolated so that the product CC^{-1} approaches one. By contrast, the choice $\alpha = \frac{1}{10}$ suggested by boundary-layer models gives instead an unacceptable sequence. The final entries in each column of the corresponding Neville tables are

0.93290699, 0.93547394, 0.93874088, 0.94216705, 0.94540554,
0.94823153, 0.95049938, 0.95211672, 0.95302919, ...,

0.318139720, 0.312279193, 0.307439847, 0.303436312, 0.300125744,
0.297395381, 0.295154678, 0.293329999, 0.291860851, ...

An independent unpublished analysis by S. N. Curle provides another sequence of numbers for estimating the value of the exponent. If an infinite series with coefficients c_n and its associated inverse d_n in x has a dominant singularity at x_0 with exponent α, then by simple manipulation one gets

$$\phi_n = -(n\pi)^2 (x_0)^{2n} c_n d_n = \alpha\pi \sin\alpha\pi.$$

This inverts to give

$$(\alpha\pi)^2 = \phi_n + \tfrac{1}{6}(\phi_n)^2 + \ldots.$$

This last equation is used to find the following sequence of numbers for α:

0.0414342457, 0.0495932504, 0.0529158314, 0.0546254786, 0.0562106034,
0.0565879831, 0.0568257415, 0.0569720611, 0.0570563920, 0.0570976316,
0.0571083778, 0.0570972908, 0.0570704735, 0.0570323152,
0.0569860261, ...

Although this sequence and that obtained previously by taking the logarithmic derivative appear similar, upon closer inspection one notices that they differ in the fourth significant figure throughout. As a result, at least within two significant figure accuracy, the above sequence again converges to a value close to $\frac{1}{18}$.

The method of Padé approximants (Baker 1965) has been applied to the original

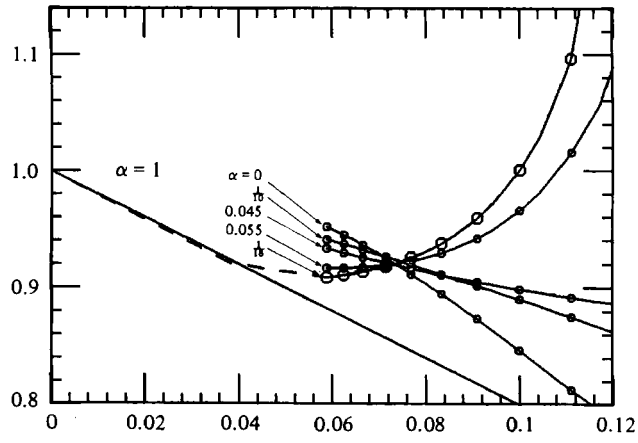

FIGURE 7. Domb–Sykes plot for flux-ratio series after Euler transformation and multiplicative extraction of the singularity with various exponents, versus $1/n$.

series. Applying Padé approximants to the logarithmic derivative gives the following sequence of numbers for the corresponding boundary-layer exponent:

$$0.0515199165,\quad 0.0565685186,\quad 0.0572354234,\quad 0.05723571836,$$
$$0.0582652476,\quad 0.0525516550,\quad 0.0544958708,\quad \ldots.$$

It is typical of Padé approximants that this sequence is irregular. However, it is very unlikely that it approaches the value $\frac{1}{10}$ of existing boundary-layer analysis, and very plausible that it approaches $\frac{1}{18}$.

4. The secondary singularity at $K = \infty$

We see that the dominant singularity at ∞ is probably a multiple of $(1-\delta)^{\frac{1}{18}}$ for the Eulerized flux-ratio series (3.22). We next multiplicatively extract this singularity, recasting the flux-ratio series as

$$\frac{f_r}{f_s} = (1-\delta)^{\frac{1}{18}} \sum_{1}^{\infty} e_n \delta^n. \tag{4.1}$$

The first 17 coefficients e_n are listed in table 1.

The Domb–Sykes plot of the new coefficients has an interesting behaviour. The study of this may lead to better understanding of the nature of the singularity. We attempt to understand this behaviour by computing the corresponding coefficients of (4.1) as a result of varying the exponent of $1-\delta$ about the value $\frac{1}{18} = 0.05555$. Figure 7 is the Domb–Sykes plot of this attempt. An interesting development occurs close to $\alpha = \frac{1}{18}$. The plot for $\alpha = 0.055$ goes to ∞ near $1/n = 0.2$, whereas that for $\alpha = 0.060$ is bounded. This behaviour for $\alpha = \frac{1}{18}$ convinces the author that this value indeed represents the correct exponent for the boundary-layer singularity. It is anticipated that, when the proper singularity is extracted, the coefficients of the remaining series will be small and of the same sign. This will occur close to the value of the exponent for which the last coefficient is zero. As can be seen this happens at about $\alpha = \frac{1}{18}$.

Figure 8 is a simplified form of figure 7, comparing the extraction of $\alpha = \frac{1}{18}$ and $\alpha = \frac{1}{10}$. If we extract the singularity with the correct exponent, the remaining series

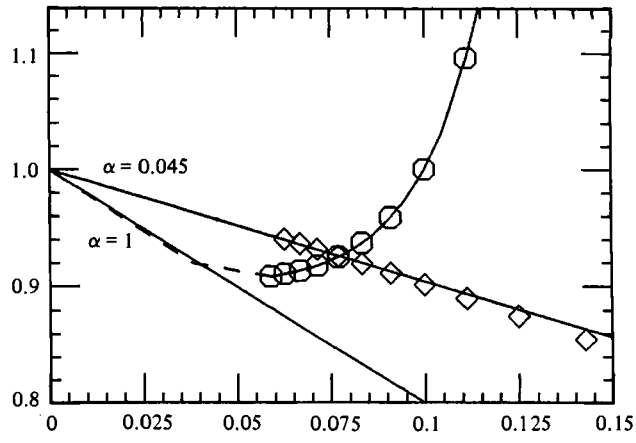

FIGURE 8. Domb–Sykes plot for flux = ratio series after Euler transformation and multiplicative extraction of the singularity with exponents $\alpha = \frac{1}{10}$ versus $1/(n-1)$ ($\diamond$) and $\alpha = \frac{1}{18}$ versus $1/n$ ($\circ$).

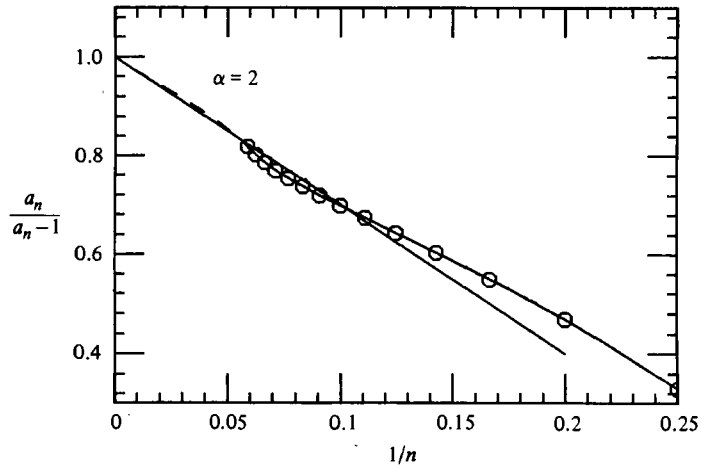

FIGURE 9. Domb–Sykes plot for flux-ratio series after Euler transformation and multiplicative extraction of dominant singularity and subtraction of logarithmic singularity.

will show a weaker coincident singularity. This has apparently occurred with $\alpha = \frac{1}{18}$, where the exponent of the secondary singularity is increased by about one. On the other hand, if we extract too large an exponent, the remaining series will offset our error by showing a compensating negative exponent. For $\alpha = \frac{1}{10}$ the secondary exponent is about -0.045, suggesting again that the correct exponent is about $\frac{1}{10} - 0.045 = 0.055$.

Furthermore, figure 8 leads to the conclusion that the secondary singularity at one has the exponent $\alpha = 1$. Such a non-negative integral value indicates that a logarithmic term intervenes. In this case the term is a multiple of $(1-\delta)\log(1-\delta)$. Therefore, estimating its coefficient, we have

$$\frac{F_r}{F_s} = C(1-\delta)^{\frac{1}{18}}\left(1 - \tfrac{1}{30}(1-\delta)\log(1-\delta) + \sum_1^\infty f_n \delta^n + \ldots\right), \tag{4.2}$$

where the first 17 coefficients f_n are listed in table 1. A new Domb–Sykes plot (figure 9) is well behaved, and oscillates around the line corresponding to the exponent $\alpha = 2$.

This indicates that a higher-order logarithmic term is involved. Thus we estimate

$$\frac{F_r}{F_s} = C(1-\delta)^{\frac{1}{18}}\Big(1-\tfrac{1}{30}(1-\delta)\log(1-\delta)-\tfrac{2}{25}(1-\delta)^2\log(1-\delta)+\sum_1^\infty g_n\delta^n\Big), \quad (4.3)$$

where the first 17 coefficients g_n are listed in table 1. A new Domb–Sykes plot oscillates too much to be relied upon. The value of C can be calculated by summing (4.3) after completing it according to (4.2), which gives $C = 1.01632$. Therefore we recast the series finally as

$$\frac{F_r}{F_s} = 1.01632(1-\delta)^{\frac{1}{18}}\Big(1-\tfrac{1}{30}(1-\delta)\log(1-\delta)-\tfrac{2}{25}(1-\delta)^2\log(1-\delta)+\sum_1^\infty g_n\delta_n\Big). \quad (4.4)$$

All the evidence, taken together, supports a value for $\alpha \approx \frac{1}{18}$. Without the benefit of any further information, we could be led to accept a value close to $\frac{1}{18}$, rational or irrational. However, asymptotic analysis in terms of conventional boundary-layer theory supports a simple rational number as a suitable choice for the exponent. Giving this argument, we conclude that $\alpha = \frac{1}{18}$ and certainly not $\frac{1}{10}$.

5. Comparison with other results for friction ratio

Itō & Nanbu (1970) introduced an alternative for the similarity parameter K that is more useful in experiments and in their boundary-layer theory. It is based on the actual mean velocity W_m down the pipe. Their k is defined in our terms as

$$k = \frac{2W_m a}{\nu}\frac{4\Omega a^2}{\nu}. \quad (5.1)$$

Since the actual flux through the rotating pipe is given by $F_r = \pi a^2 W_m$, then

$$F_r = \frac{\pi n^2}{8\Omega a}k. \quad (5.2)$$

The K that we have used is based on the hypothetical mean velocity W_0, or equivalently on the pressure gradient

$$K = \frac{W_0 a}{\nu}\frac{2\Omega a^2}{\nu}. \quad (5.3)$$

For a parabolic profile, the mean velocity is half of the maximum, so the flux rate is

$$F_s = \tfrac{1}{2}\pi a^2 W_0 = \tfrac{1}{4}\pi\frac{\nu^2}{a\Omega}K. \quad (5.4)$$

From (5.4) and (5.2)

$$\frac{F_r}{F_s} = \frac{k}{2K}. \quad (5.5)$$

Values of the friction ratio $f_r/f_s = (F_r/F_s)^{-1}$ are given by our flux-ratio series (4.1). In terms of Itō's parameter k, the flux-ratio series (3.11) converges up to $k \approx 790$. To compare with the boundary-layer analysis, we also convert our asymptotic expression to Itō's parameter k. The flux ratio decreases as $1.01631(1-\delta)^{\frac{1}{18}}$. In terms of the original variable K then,

$$\frac{F_r}{F_s} \sim 1.98483K^{-\frac{1}{9}} \quad \text{as} \quad K\to\infty. \quad (5.6)$$

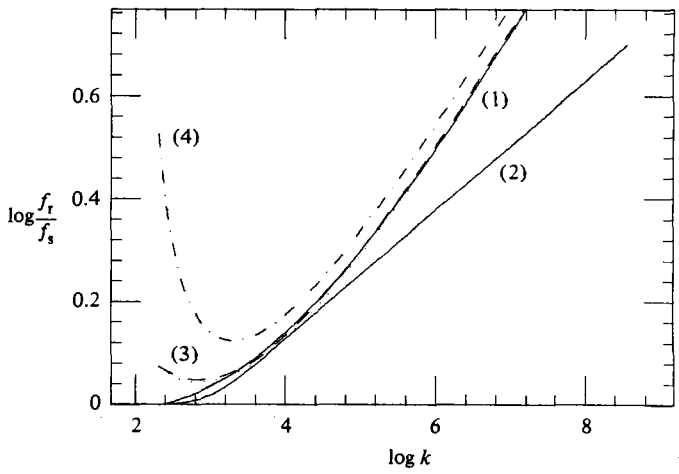

FIGURE 10. Friction ratio for laminar flow in slowly rotating pipe: (1) Itō's experiment; (2) present theory; (3) Itō's boundary layer, (4) Mori & Nakayama's boundary layer.

Comparing (5.5) with (5.6) yields the asymptotic relationship between our parameter and Itō's:

$$k = 3.96967K^{\frac{8}{9}}. \tag{5.7}$$

Hence the flux ratio decays as

$$\frac{F_r}{F_s} \sim 2.01933k^{-\frac{1}{8}}, \tag{5.8}$$

and the friction ratio grows asymptotically as

$$\frac{f_r}{f_s} = \left(\frac{F_r}{F_s}\right)^{-1} \sim 0.49521k^{\frac{1}{8}}, \tag{5.9}$$

Figure 10 is a comparison of previous experimental and boundary-layer results with the semi-numerical result obtained in this research.

6. Discussion

A major difference between our results and those of previous analyses is in the asymptotic behaviour of the friction factor as the similarity parameter $K = RR_r$ and hence k increases. The prevailing opinion has been that the relationship goes as $f_r/f_s \sim k^{\frac{1}{4}}$, whereas we find that $f_r/f_s \sim k^{\frac{1}{8}}$.

As can be seen in figure 10, this difference is not significant until k is greater than 30000. Below that there is little discrepancy between the present work and others. It can be explained by the fact that experiments require a finite amount of rotation, whereas this investigation considers the limit as the rotational Reynolds number goes to zero. It would be helpful to obtain experimental data for this rotating-pipe problem when R_r is very small in order to see if our analysis is valid for considerably lower values of k.

As regards the difference between the asymptotic behaviours for large values of k, $f_r/f_s \sim k^{\frac{1}{8}}$ versus $f_r/f_s \sim k^{\frac{1}{4}}$, the following remarks can be made.

(*a*) Our expansion is based on the double limit

$$\left.\begin{matrix} R_r \to 0, \\ R \to \infty, \end{matrix}\right\} \quad K = RR_r \text{ fixed.}$$

From an expansion for small K the limiting case as K goes to infinity has been extracted; however, the experiments are based upon $R \to \infty$ and R_r fixed (and small). In other words the asymptotic behaviour may depend on the manner in which the similarity parameter tends to infinity.

(*b*) The uniqueness of the problem at very large values of the similarity parameter may be in question. If the solution is not unique, then there exists a bifurcation, one solution being observed and the other one might conform with present theory. In the similar flow through a curved pipe, Taylor (1929) expressed the possibility that there may exist an intermediate flow regime between the laminar and turbulent ranges. He observed a transition from a steady laminar flow to a laminar vibrating flow as the speed increased. The onset of turbulence occurred only at a significantly higher speed.

As far as uniqueness is concerned, recently in the same class of problems a second solution has been observed. Dennis & Ng (1982) and Nandakumar & Masliyah (1982) have been able to obtain dual solutions in a coiled pipe using a series truncation and finite-difference methods respectively. The same phenomenon has also been observed in the flow through a curved semicircular duct (see Masliyah 1980). By existence of such a duality, the fact (which has long been established) that the laminar flow in a curved duct is composed of a main flow in the axial direction with a superimposed secondary flow having two counter-rotating vortices, should be reconsidered. Certainly the second solution having four counter-rotating vortices will raise the question about other branches of bifurcation. The same phenomenon has also been observed in the flow through a curved semicircular duct (see Masliyah 1980). Therefore there is a possibility that at high K the experiments show one of those branches.

Thus we have seen possible explanations for the discrepancy between our semi-numerical results and the experiments regarding the exponent of the similarity parameter. For large values of $K = RR_r$, however, conventional boundary-layer theories, which are based on the same equations as ours, and the same assumption of slow flow, are in agreement. So, if the experimental curves are not completely describing the flow field, then we also must find fault with the boundary-layer curves. Mori & Nakayama (1968) attempted to explain what is happening in the boundary layer and core at high values of k. They reasoned that, since the flow is fully developed, the thickness δ of the boundary layer is constant in the direction of the pipe axis, but varies with angle Θ. Then they made the assumption that the thickness of the boundary layer is independent of the angular coordinate, and therefore can be treated as a constant. As previously mentioned in §1, because of the direction of the Coriolis force there is no symmetry, so this assumption seems to be inconsistent. Based on what has already been shown, Itō's model for the structure of the flow leads to the result that in the vicinity of the innermost point the boundary-layer thickness is infinite; or, in other words, his model breaks down locally.

The question now arises as to whether or not the present semi-numerical results can be used to correct the boundary-layer model. Although we have analysed local quantities at a few points, it would be very tedious to calculate in this way the whole flow field for large K.

As far as we know, there is one finite-difference solution by Duck (1983) corres-

Powers of $K = RR_r$	Powers of R_r^2				
	0	1	2	3	4
0	$n = 1$	$n = 2$	$n = 3$	$n = 4$	$n = 5$
1	$n = 2$	$n = 3$	$n = 4$	$n = 5$	
2	$n = 3$	$n = 4$	$n = 5$		
3	$n = 4$	$n = 5$			
4	$n = 5$				

TABLE 2. Powers of $K = RR_r$ and R_r^2 in nth approximation of double expansion

ponding to low values of K for our rotating-pipe problem. In general, finite-difference approaches to our problem are inadequate, because an impractically fine mesh would be required to give the right structure for very high values of the similarity parameter $K = RR_r$.

Appendix. Distinguished limits for slowly rotating pipe

Equations (2.1) and (2.2) are seen to involve two parameters RR_r and R_r^2. A double expansion of the solution would contain the powers of these quantities listed in table 2. The resulting series for the friction ratio would contain, by symmetry, only the even powers of K:

$$\frac{f_r}{f_s} = 1 + 256\left(\frac{R_r}{768}\right)^2 + \frac{1}{7}\left(\frac{RR_r}{768}\right)^2 + \ldots. \tag{A 1}$$

(Barua's equation (21) contains these same two combinations, but with different coefficients because he uses a different definition of friction ratio.)

Such a double expansion is expensive to compute, and methods of analysing double power series are not well developed. One way of reducing it to a single expansion is to fix the value of R_r. Instead, we suppose that R_r is small; then a first approximation contains terms from only the first column of table 2. This corresponds formally to the double limit adopted in §3.

Furthermore, the author anticipated (as has happened in some other problems) that the coefficients in successive columns of table 2 decrease in magnitude (for low values of R_r).

We suggested in §6 that our solution differs from experiment because we let R_r tend to zero, whereas in experiment it is fixed. We propose the following suggestion for improving the theory. We do not neglect R_r, but assume (with $K = RR_r$) the relation

$$(R_r)^2 = \delta K^\beta,$$

for some exponent β, where δ is a constant of order unity (but presumably smaller than one). Then the axial-momentum equation (which is the only place that R_r appears in the problem) becomes

$$\nabla^2 W + 4 = -K\left(\frac{\partial \Psi}{\partial r}\frac{\partial W}{\partial \Theta} - \frac{\partial \Psi}{\partial \Theta}\frac{\partial W}{\partial r}\right) + \delta K^\beta \left(\sin\Theta \frac{\partial \Psi}{\partial r} + \cos\Theta \frac{\partial \Psi}{\partial r}\right). \tag{A 2}$$

The limiting form of the equation for $K \to 0$ changes from the Poiseuille equation $\nabla^2 W + 4 = 0$ for $\beta > 0$ to the degenerate form $(\cos\Theta)\,\partial\Psi/\partial r - (\sin\Theta/r)\,\partial\Psi/\partial\Theta = 0$ for $\beta < 0$, or at $\beta = 0$ to

$$\nabla^2 W + 4 = \delta\left(\sin\Theta \frac{\partial \Psi}{\partial r} + \frac{\cos\Theta}{r}\frac{\partial \Psi}{\partial \Theta}\right). \tag{A 3}$$

This is a distinguished limit in the sense of Cole (1968). However, it is difficult to solve this equation in simple closed form, as we can the Poiseuille equation, to start an expansion in powers of K. That difficulty disappears if we take $\beta = 1$, which is also a distinguished limit from the point of view of higher approximations. For both terms on the right-hand side of (A 2) are of the same order in K, and hence equally small. We may say that $\beta = 1$ gives a distinguished second-order limit. Equation (A 2) becomes

$$\nabla^2 W + 4 = -K\frac{1}{r}\left(\frac{\partial \Psi}{\partial r}\frac{\partial W}{\partial \Theta} - \frac{\partial \Psi}{\partial \Theta}\frac{\partial W}{\partial r}\right) + \delta K\left(\sin\Theta\frac{\partial \Psi}{\partial r} + \frac{\cos\Theta}{r}\frac{\partial \Psi}{\partial r}\right).$$

Then when we expand the solution in powers of K,

$$W = W_1 + KW_2 + K^2 W_3 + \ldots,$$
$$\Psi = \Psi_1 + K\Psi_2 + K^2\Psi_3 + \ldots,$$

the second-order equation becomes

$$\nabla^2 W_2 = -\frac{1}{r}\left(\frac{\partial \Psi_1}{\partial r}\frac{\partial W_1}{\partial \Theta} - \frac{\partial \Psi_1}{\partial \Theta}\frac{\partial W_1}{\partial r}\right) + \delta\left(\sin\Theta\frac{\partial \Psi_1}{\partial r} + \frac{\cos\Theta}{r}\frac{\partial \Psi_1}{\partial \Theta}\right).$$

This is a 'richer' equation than the one with $\delta = 0$ that the present work solves at this stage.

In the same way we say that $\beta = 2$ gives a distinguished third-order limit; the equations for W_1 and W_2 are the same as in the present work, but those for W_3 and higher terms are richer. But we gain the most information from the smallest value of β.

It would be interesting to repeat the computations of this paper for the distinguished limit with $\beta = 1$. It is to be hoped that this would lead us to explain better the flow field.

The author is indebted to Professor M. D. Van Dyke for his encouragement and valuable advice during the course of this research. Support was provided by the Air Force Office of Scientific Research under contract AFOSR 74–2649 and National Science Foundation contract CME-7824412.

REFERENCES

ADLER, M. 1934 Strömung in gekrümmten Rohren. *Z. angew. Math. Mech.* **5**, 257–273.

BAKER, G. A. 1965 The theory and application of the Padé approximant method. In *Advances in Theoretical Physics* (ed. K. A. Brueckner), vol. 1, pp. 1–58. Academic.

BARUA, S. N. 1954 Secondary flow in a rotating straight pipe. *Proc. R. Soc. Lond.* A **227**, 133–139.

BENNETS, D. A. & HOCKING, I. M. 1974 Pressure-induced flows at low Rossby numbers. *Phys. Fluids* **17**, 1671–1676.

BENTON, G. S. 1956 The effect of the Earth's rotation on laminar flow in pipes. *J. Appl. Mech.* **23**, 123–127.

COLE, J. D. 1968 *Perturbation Methods in Applied Mathematics.* Blaisdell.

DEAN, W. R. 1927 Note on the motion of fluid in a curved pipe. *Phil. Mag.* (7) **4**, 208–223.

DEAN, W. R. 1928 The stream-line motion of fluid in a curved pipe. *Phil. Mag.* (7) **5**, 673–695.

DENNIS, S. C. R. & NG, M. C. 1982 Dual solution for steady laminar flow through a curved tube. *Q. J. Mech. Appl. Maths* **35**, 305–324.

DUCK, P. W. 1983 Flow through rotating pipes of a circular section. *Phys. Fluids* **26**, 614–618.

GAUNT, D. S. & GUTTMANN, A. J. 1974 Series expansions: analysis of coefficients. In *Phase Transitions and Critical Phenomena* (ed. C. Domb & M. S. Green), vol. 3, pp. 181–243. Academic.

ITŌ, H. & MOTAI, T. 1974 Secondary flow in a rotating curved pipe. *Rep. Inst. High Speed Mech.* **29**, 33–57.

ITŌ, H. & NANBU, K. 1971 Flow in rotating straight pipes of circular cross-section. *Trans. ASME* D: *J. Basic Engng* **93**, 383–394.

JONES, J. R. & WALTERS, T. S. 1967 A note on the motion of a viscous liquid in a rotating straight pipe. *Z. angew. Math. Phys.* **18**, 774–781.

MASLIYAH, J. H. 1980 On laminar flow in curved semicircular ducts. *J. Fluid Mech.* **99**, 469–479.

MORI, Y. & NAKAYAMA, W. 1968 Convective heat transfer in rotating radial circular pipes (1st Report, laminar region). *Intl J. Heat Mass Transfer* **11**, 1027–1040.

NANDAKUMAR, K. & MASLIYAH, J. H. 1982 Bifurcation in steady laminar flow through curved tubes. *J. Fluid Mech.* **119**, 475–490.

TAYLOR, G. I. 1929 The criterion for turbulence in curved pipes. *Proc. R. Soc. Lond.* A **124**, 243–249.

TREFETHEN, L. 1957*a* Fluid flow in radial rotating tubes. In *Actes*, 9 *ème Congr. Intle de Méc. Appl.*, vol. 1, pp. 341–350. Université de Bruxelles.

TREFETHEN, L. 1957*b* Flow in rotating radial ducts: report R55GL 350 on laminar flow in rotating, heated horizontal, and bent tubes, extended into transition and turbulent regions. *Gen. Elec. Co. Rep.* 55GL350-A.

VAN DYKE, M. 1970 Extension of Goldstein's series for the Oseen drag of a sphere. *J. Fluid Mech.* **44**, 365–372.

VAN DYKE, M. 1974 Analysis and improvement of perturbation series. *Q. J. Mech. Appl. Maths* **27**, 423–450.

VAN DYKE, M. 1975 Computer extension of perturbation series in fluid mechanics. *SIAM J. Appl. Maths* **28**, 720–734.

VAN DYKE, M. 1978 Extended Stokes series: laminar flow through a loosely coiled pipe. *J. Fluid Mech.* **86**, 129–145.

WHITE, C. M. 1929 Streamline flow through curved pipes. *Proc. R. Soc. Lond.* A **123**, 645–663.